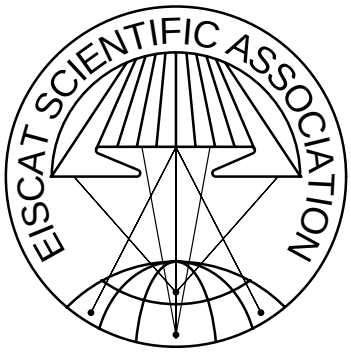

EISCAT TECHNICAL NOTE

A MORPHOLOGICAL STUDY OF THE INTEGRATED TOTAL ELECTRON CONTENT AND F REGION PARAMETERS USING EISCAT IN THE FRAME OF SPACE WEATHER

by

J. Lilensten, B. Pibaret, B. Lemieux-Dudon

Laboratoire de Planétologie de Grenoble
Observatoire des Sciences de l'Univers de Grenoble
Bâtiment D de physique, B.P. 53
F-38041 Grenoble cedex 9, France

KIRUNA
Sweden

A morphological study of the Integrated Total Electron Content and F region parameters using EISCAT in the frame of Space Weather

J. Lilensten, B. Pibaret, B. Lemieux-Dudon

Laboratoire de Planétologie de Grenoble
Observatoire des Sciences de l'Univers de Grenoble
Bâtiment D de physique, B.P. 53
38041 Grenoble cedex 9

EISCAT Technical Report 04/54
EISCAT Scientific Association

EISCAT Scientific Association
PO Box 164
SE 981 23 Kiruna, Sweden
March 2004
EISCAT Technical Report 04/54
ISSN 0349-2710

A morphological study of the Integrated Total Electron Content and F region parameters using EISCAT in the frame of Space Weather

J. Lilensten, B. Pibaret, B. Lemieux-Dudon
Laboratoire de Planétologie de Grenoble
Observatoire des Sciences de l'Univers de Grenoble
Bâtiment D de physique, B.P. 53
38041 Grenoble cedex 9

Abstract

EISCAT has been extensively used as a unique tool for ionospheric research studies. Nowadays, EISCAT appears to be also an important facility in the frame of the Space Weather studies. In particular, the Total Electron Content and foF2 parameters at high latitude are required parameters in Space Weather that EISCAT can provide. This report presents an overview of the different behaviour of this parameters deduced from EISCAT measurements. We study the behaviour of these parameters at different solar activity levels, their changes under particle precipitation, geomagnetic storms, and arcs. We make use of the EISCAT (European Incoherent SCATter) data processed in Grenoble over more than one solar cycle.

In the conclusion, we underline that this study resulted from an update of the EISCAT data base and a recommendation of the international ITU-R committee to use EISCAT as a Space Weather facility.

Introduction

The ionosphere and thermosphere have important impacts on several branches of technology. Most of the telecommunication signals travel through or are reflected by the ionosphere. Low altitude spacecraft orbit in the thermosphere. Both telecommunications and spacecraft's are therefore sensitive to any perturbation in their environment. Unfortunately, very few parameters are routinely measured on a large scale: only the ionospheric Total Electron Content (TEC) and the F-region maximum parameters: height, hmF2 and electron density (or frequency foF2) may be accessible. Usually, they are estimated from dual frequency GPS observations (Iijima et al., 1999 and references therein) and from ionosonde data.

For the last 30 years, a great deal of effort has been spent in modelling those parameters (see for example Rush et al., 1974; Kouris et al., 1998; Codrescu et al., 1999) and, in the frame of the space weather activities, to forecast them (Altinay et al., 1997). Amongst international codes, one can mention the International Reference Ionosphere (IRI) (Bilitza, Papitashvili, King, 2001 and references therein) and the model developed under the auspice of the COST 251 Action "Improved Quality of Service in Ionospheric Telecommunication Systems Panning and Operations" called COSTprof (Stanislawska et al., 1998). Different approaches are made to invert them in order to retrieve full profiles (see for example Komjathy et al., 1998).

The high latitude ionosphere can be considerably altered in composition and structure by the various physical processes:

- Particle precipitation is superimposed on photon fluxes in the ionization and heating processes; during night-time periods, these charged particles are the only production source;

- Field aligned currents (a few A m-2) are sources of energy transport (diffusive heat flow) for the thermal plasma. Depending on their upward or downward direction, they can heat or cool the thermal electron gas respectively. Then, they generate ponderomotive forces, which trigger the vertical motion of plasma (Wahlund et al., 1992);

- The convection electric field (up to 200 mV m-1) is responsible for the E×B plasma drift. As a consequence, a particular plasma tube crosses different regions of the ionosphere (trough, night side, or dayside,) and is connected to different regions of the magnetosphere characterized by sources of particles of different energy ranges (Newell and Meng, 1994).

Thus, models often fail to retrieve the high latitude ionosphere (Jakowski et al., 1996, 1998). EISCAT turns to be a milestone facility to help fix this problem. It has been operating for more than a solar cycle, and thus provides a record particularly well suited to "space climatology". Its new system allows real time measurements that are often necessary for Space Weather purposes.

The purpose of this technical report is to make use of the 18 years of EISCAT data processed in Grenoble in order to make a study of the behaviour of the TEC and F region parameters over a full solar cycle. We do not intend to make a full statistical study, which will be the goal of further study. We aim at underlining the use of EISCAT in Space Weather studies.

Following this work, the EISCAT database has been expanded with the TEC and F region parameters. Moreover, the International Telecommunication Union Radiocommunication group (ITU-R) on « Ionospheric propagation data and prediction methods required for the design of satellite services and systems » issued a recommendation to use EISCAT for Trans-ionospheric model testing. This will be discussed at the end of this report.

The ITEC and F region parameters above EISCAT

We make use of the 1983-1994 data, spanning a full solar cycle. We consider the experiments that include the measurement of the electric field. This is important if one wants to distinguish the effects of precipitation and of the electric field. The data are processed with one to five minutes integration, which is sufficient for our purpose. All the data have been reprocessed in Grenoble with the TAPANAL data processing code (Lathuillère and Pibaret, 1992).

We focus on the CP1 EISCAT mode experiments. In this mode, the Tromsø antenna is fixed parallel to the magnetic field. The remote sites make continuous measurements at the F-region height (typically at 278.6 km). We do not use other EISCAT mode experiments, when the Tromsø antenna moves. The reason is that in these other modes, one cycle may last up to 20 minutes, from which only the B-parallel position could be fully usable for our purposes. Within 20 minutes, the ionospheric characteristics can change drastically and introduce uncertainties into our observations. Finally, we only select experiments lasting at least 12 hours.

The number of such CP1 experiments with electric field measurement amounts to 31 only, covering 64 days and 1260 hours. This shows the difficulty of ionospheric experiments, and the impossibility to perform a full statistical study of the behaviour of high latitude parameters. Therefore, we will only show the most prominent features.

From those measurements, it is possible to compute the electron content up to 425 km and the F region parameters. This upper limit may seem rather low compared to the capability of the EISCAT radar (usually at least 600 km). It comes from the fact that we want to examine the behaviour of the electron density. The best parameter in this case is the corrected power profile, which goes from 90 to 425 km with a resolution of 3 km, better than the 21 km resolution in the F region obtained in the single pulse mode.

The TEC values usually used for communication applications are deduced from GPS measurements and represent a summation of all the electrons up to 22 000 km, much higher than can be reached with the EISCAT radar. Therefore, we cannot draw any conclusion on the absolute values of the electron content with the radar data. However, the TEC integrated up to 425 km represents roughly half of the total integrated TEC (Lilensten and Blelly, 2002). Moreover, the largest effects of particle precipitation and electric fields are in the E and F regions of the ionosphere, which are covered by the radar. Then, it is possible to make a study of the relative behaviour of the total electron content with the radar data. In order to distinguish between the usual Total Electron Content up to 22000 km and the Total Electron Content integrated up to a lower altitude, the first is called TEC and the second ITEC (the I stands for Integrated). When an ambiguity occurs, the upper altitude of integration may be added as an index.

Figure 1 shows an experiment conducted in November 1987 during quiet solar conditions and quiet magnetic conditions. In the top panel, we show the total electric field in $mV.m^{-1}$.

The two panels below show respectively the $f_{10.7}$ decimetric flux and the 3 hourly Ap index. The Ap index is of course a planetary index, which should not be used as a parameter in a parameterization of the ITEC quantity. Instead, it has been shown by Mikhailov and Mikhailov (1995) that a pertinent index MF2 should be used in order to provide the best critical frequency of the F2 layer versus solar activity. But this is a monthly index not suitable for the daily F-layer parameter variation considered in this paper. A study of the correlation between time varying indexes and the high latitude ionosphere can be found in Perrone and Franceschi, 1999. The problem of TEC relationship with indexes of solar and geomagnetic activities has been discussed in several publications (e.g. Das Gupta et al., 1975; McNamara and Wilkinson, 1983; Jakowski et al, 1991) and will not be further discussed here.

We then plot the solar zenith angle SZA and finally, in the bottom panels, the altitude of the F2 peak (hmF2), its density value (NmF2), and the ITEC integrated from 90 to 425 km.

We will study the effects of different parameters on a selected choice of experiments, illustrating a general behaviour. All the studied experiments are available online at the same EISCAT database website. In the results presented here, all ITEC values are in electron per square meter unit. In the plots, we have chosen to use the TEC unit (sometimes refereed as TECU), which is equal to 10^{16} electrons per square meter.

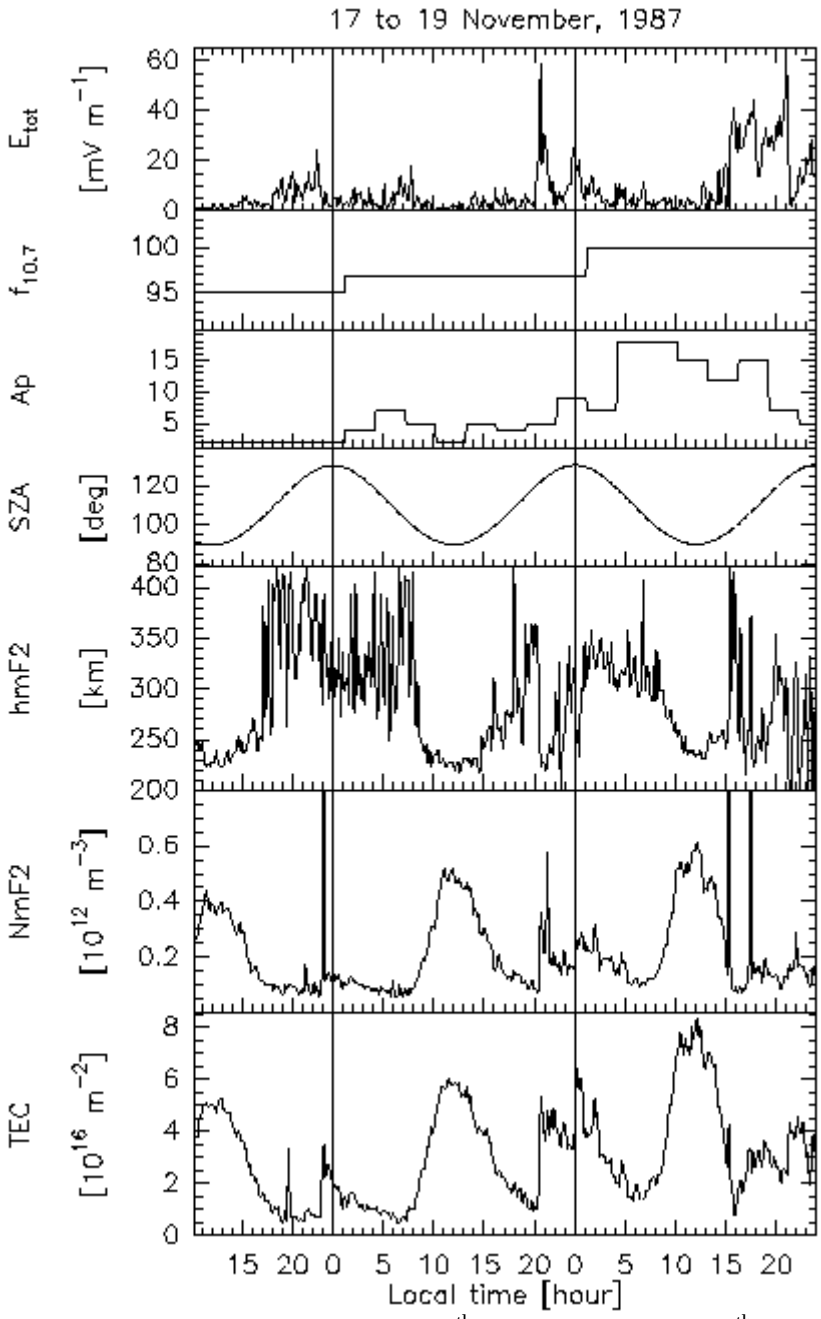

Figure 1: The EISCAT experiment from the 17th November to the 19th November 1987. The hours are local time. The straight vertical lines indicate midnight. In the upper panel, we plot the total electric field in mV m^{-1}. The three panels below show respectively the $f_{10.7}$ index, the Ap index, and the solar zenith angle in degrees. Below is the altitude of the F2 peak (hmF2) in km, the electron density at hmF2 (NmF2) and the total electron content integrated up to 425 km.

Daytime experiments: effect of the EUV solar flux

Effects of solar EUV flux on the ionosphere can be seen in the experiment carried out during the period November 17–19, 1987 (Figure 1). The solar zenith angle takes values slightly smaller than 90° at noon. The solar conditions are quiet, $f_{10.7}$ taking the values of 95, 97, and 100. The magnetic conditions are quiet too (Ap ranges between 2 and 17), with no electric field at noon. This allows separation of the effect of the sole solar photoionization and other sources for the electron production. The ITEC and NmF2

parameters experience an increase which follows $f_{10.7}$ at noon, the ITEC values are respectively 5 10^{16}, 6 10^{16}, and 8 10^{16} m^{-2}. The altitude of the F maximum is 220 km for the first two days at noon, and reaches 240 km the third day.

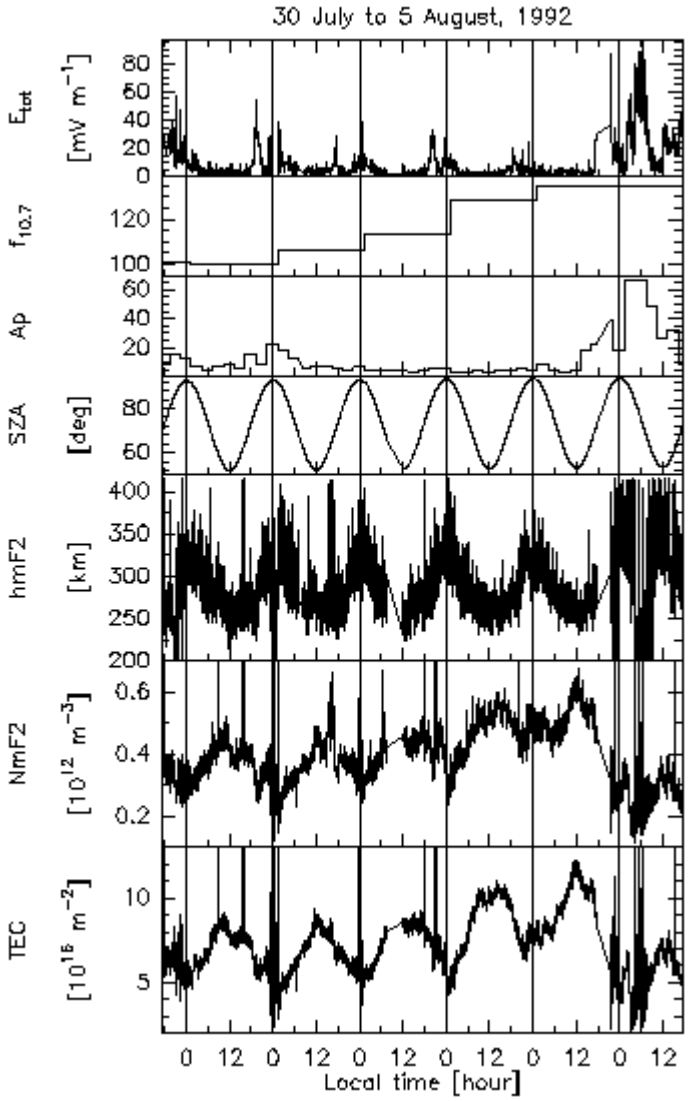

Figure 2: Same as Figure 1 for the experiment from the 30 July to the 5 August 1992.

Several other experiments exhibit the same behaviour. The July 30th to August 5th 1992 (Figure 2) experiment has a slightly higher solar activity, with $f_{10.7}$ increasing from 100 to 134. The electric field remains small, and there is no evidence of a magnetic storm. The values of the noon ITEC are respectively 9, 9, 10, 10.8, and 11.8 10^{16} m^{-2}.

At higher solar activity level, 30th to 31st March 1992 (not shown here), the $f_{10.7}$ index increases from 182 to 191, with a noon ITEC varying from 24 10^{16} to 28.5 10^{16}. Finally, the November 14th to 16th, 1989 (Figure 3) observations were made during high solar activity levels: $f_{10.7}$ varies from 243 to 217. There, the noon ITEC varies from 34 10^{16} to 24 10^{16}. This last experiment can be compared to the experiments held in the same period of the year (17th to 19th November 1987, shown in Figure 1). The magnetic activity is quiet for the two experiments (kp ranges between 5 and 15) and except for short periods,

the electric field remains low (less than 10 $mV.m^{-1}$). Only the solar activity is very different between the 1987 experiment ($f_{10.7}$ = 95-100) and 1989 ($f_{10.7}$ > 210). HmF2 is lower at low solar activity (225 km at noon to 340 at midnight) than at high solar activity (300 km at noon to 420 at midnight).

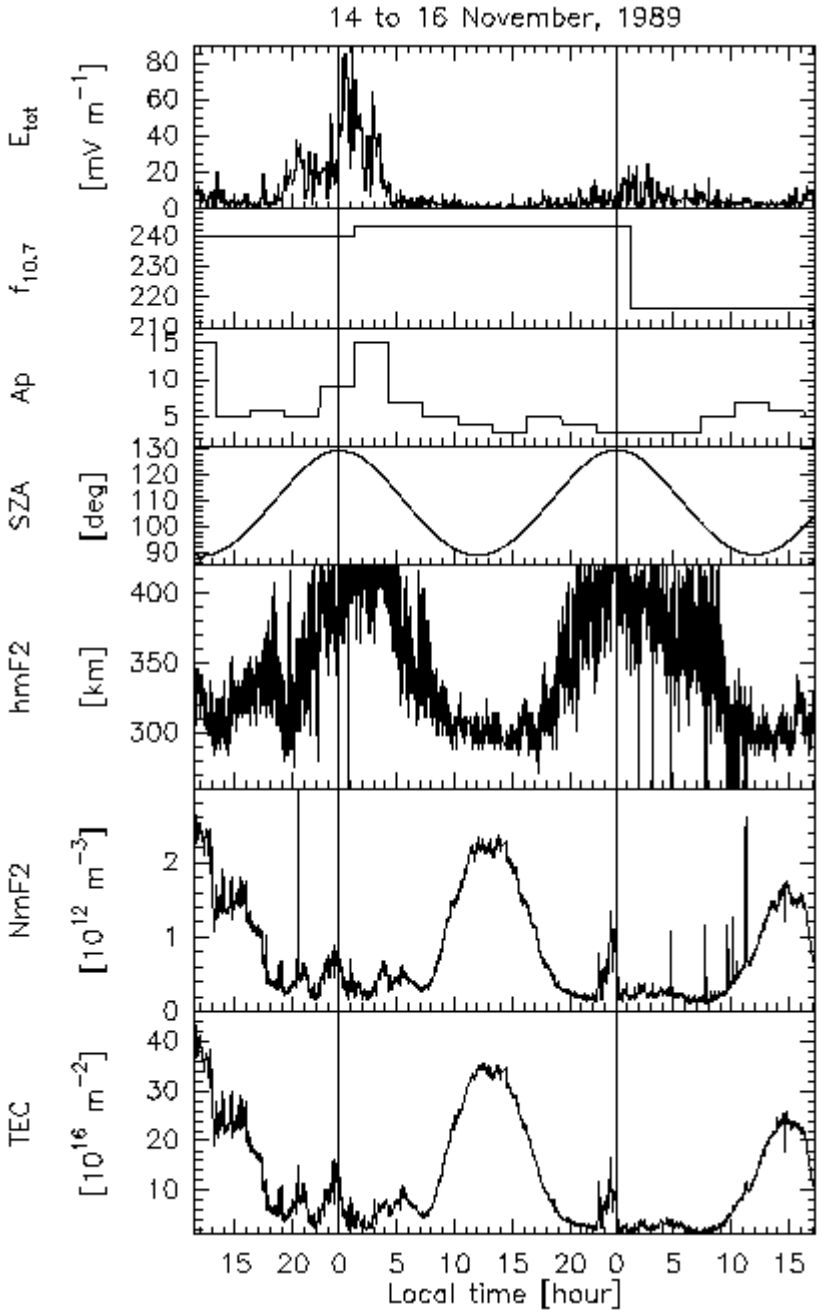

Figure 3: Same as Figure 1 for the experiment held from the 14 to the 16 November 1989

In order to characterize the Total Electron Content versus the solar index, one makes the following approach: adopting the continuity equation for the ionospheric electrons, we have

$$\frac{dN_e}{dt} = q - L_e - \mathrm{div}(N_e \mathbf{v}) \qquad (1)$$

where q is the electron production due to the solar EUV radiation, N_e is the electron density, L_e the electron loss term and **v** the electron velocity. We have no way to control the transport term (the divergence term of equation 1). During quiet magnetic periods, we can assume that it will probably be of minor importance, especially in the E- and lower F-region because the recombination loss rates are far more important here. Assuming a steady state, justifiable again for the quiet time analysis we are performing here, the loss rate will be equal to the production rate at all times, and

$$q = L_e \qquad (2)$$

We must stress that the photochemical equilibrium and the steady state assumptions should not be applied above 200 km, and that fluid and kinetic transport can only represent the physics of the F region. We use them here in order to establish a basis for the fitting procedure that we will use later.

The production maximum at a given solar zenith angle χ due to solar radiation for an atmosphere with constant scale height can be expressed as

$$q = \frac{q_o}{\text{chap}\,\chi} \qquad (3)$$

where q_o is the production for overhead sun. chap χ is a Chapman function. For low solar zenith angles (i.e. below 75°), it can be approximated by chap $\chi = \frac{1}{\cos\chi}$. At high solar angles, a more sophisticated function must be used (Chapman, 1931). Rigorously, the Chapman theory is applied only to an atmosphere ionized by a monochromatic radiation, while a wide solar spectrum ionizes the ionosphere. Again we use this formalism as a basis for the next fitting procedure.

If one discards the secondary production due to collisions between suprathermal photoelectrons and the neutral atmosphere, the production is directly proportional to the solar intensity on top of the ionosphere I_∞:

$$q \propto I_\infty / \text{chap}\,\chi \qquad (4)$$

As a first approximation, $f_{10.7}$ can be considered as proportional to the total intensity. Indeed, the modelling of the ionosphere requires the knowledge of the input flux, which is often linearly interpolated between data flux values with use of the $f_{10.7}$ index. Then:

$$q \propto f_{10.7} / \text{chap}\,\chi \qquad (5)$$

At altitudes below typically 200 km, one can expect that dissociative recombination is the dominant loss mechanism (with coefficient α), such that:

$$L_e = \alpha\ N_e^{\,2} \qquad (6)$$

In this region, we then obtain:

$$\frac{N_e}{\sqrt{f_{10.7} / \text{chap}\,\chi}} = \text{constant} \qquad (7)$$

Since the integration is a linear operation, we also have:

$$\frac{\text{ITEC}}{\sqrt{f_{10.7} / \text{chap}\,\chi}} = R1 \qquad (8)$$

where R1 is supposedly a constant. At higher altitudes, up to the lower F-region, the charge exchange between O^+ and O is important and the loss can be expressed as

$$L_e = \beta \; N_e \tag{9}$$

and we therefore get:

$$\frac{\text{ITEC}}{f_{10.7} \,/\, \text{chap}\,\chi} = R2 \tag{10}$$

where R2 is another constant. The chemical coefficients have been extensively studied in recent years (see for example Sheehan, 2001 and references therein). For specific studies, their dependence in temperature should be taken into account. This is not necessary in this study.

To study these laws, we have selected EISCAT values with solar zenith angle smaller than 90°, quiet magnetic activity (Ap < 15) and small electric fields (< 20 mV m^{-1}). We are then left with 21 056 EISCAT data points. In the following, the ITECs are in TECU.

In Figure 4, we have plotted the ratio of equation 10 versus the solar zenith angle for a Chapman function equal to 1/cosχ (upper panel) and for a Chapman function from Smithe and Smith, 1972 (bottom panel). The fact that we do not get a constant with the 1/cosχ function is not surprising. However, even with the approximated Chapman function, the ratio R2 is not constant either. This has different reasons. First, in order to establish the equation 10, we have made several assumptions that cannot reflect reality precisely. Another reason is that any Chapman function requires knowledge of the neutral atmosphere. We use the MSIS model (Hedin, 1991). However, the neutral atmosphere is still not very well reproduced by the models at high latitude. Then, using a Chapman function to calculate R2 (or R1) adds an uncertainty of which the main effect is to scatter the data points. We have tested several other expressions (Green 1964, or a direct integration) with the same results. Therefore, and in spite of its poor ability to represent the physics, we keep in the following an 1/cosχ expression for the Chapman function.

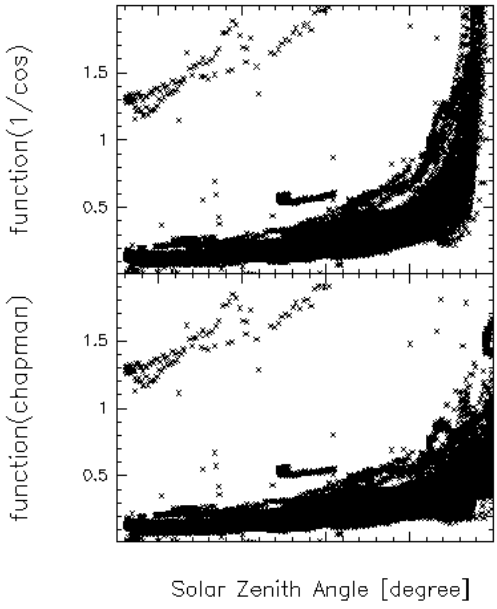

Figure 4: In the two panels, we plot the ratio R2 computed for quiet magnetic (Ap < 15) and electric (total electric field < 20 mV m^{-1}) conditions. In the upper panel, the Chapman function is approximated by 1/cosχ. In the bottom panel, a Chapman function is computed using the Smithe and Smith (1972) approach

In Figure 5, we have plotted the ratio of equation 8 versus the solar zenith angle (upper panel). The excursion of R1 at low angle is about 4, increasing with the solar angle. In the middle panel, we have plotted R2. The same pattern is seen, but now, the values are much smaller: the width of the curve is about 0.2 at small solar angles, and increases also at large angles. R2 is typically 10 times smaller than R1, showing that the ITEC behaves more like equation 10 than equation 7.

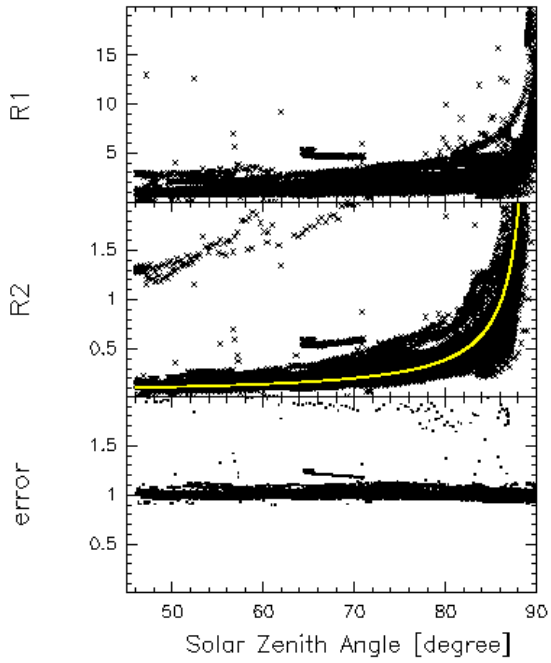

Figure 5: The upper panel shows the ratio R1 and the middle panel the ratio R2 for quiet magnetic (Ap < 15) and electric (total electric field < 20 mV m^{-1}) conditions. The Chapman function is approximated by $1/\cos\chi$ in both panels. In the middle panel, the line represents the result of the fitting procedure. The bottom panels show the error on the R2 when the approximation is used.

In order to correct the equation 10, we have fitted this curve with a hyperbolic function:

$$\hat{R}2(\chi) = \frac{1}{A}\frac{1}{\tanh(\pi/2 - \chi)} + \frac{1}{B} \qquad (11)$$

where $\hat{R}2(\chi)$ represents of course the estimate of R2. With a chi-square fitting procedure, we found A = 15.0189 and B = 166.17, with standard deviations respectively equal to 0.0547 and 2 10^{-3}. There is not much difference on $\hat{R}2(\chi)$ when A = 15 and B = 0 so that we can insure that for quiet magnetic and electric conditions,

$$\hat{R}2(\chi) = \frac{1}{15}\frac{1}{\tanh(\pi/2 - \chi)} \qquad (12)$$

In the bottom panel of Figure 5, we have plotted the ratio $R2(\chi)/\hat{R}2(\chi)$. It is remarkably constant, especially when one considers that the solar decimetric index covers values from less than 70 to more than 300. Therefore, we have the following behaviour of the ITEC above EISCAT:

$$\text{ITEC} = \frac{1}{15}\frac{f_{10.7}\cos\chi}{\tanh(\pi/2 - \chi)} \qquad (13)$$

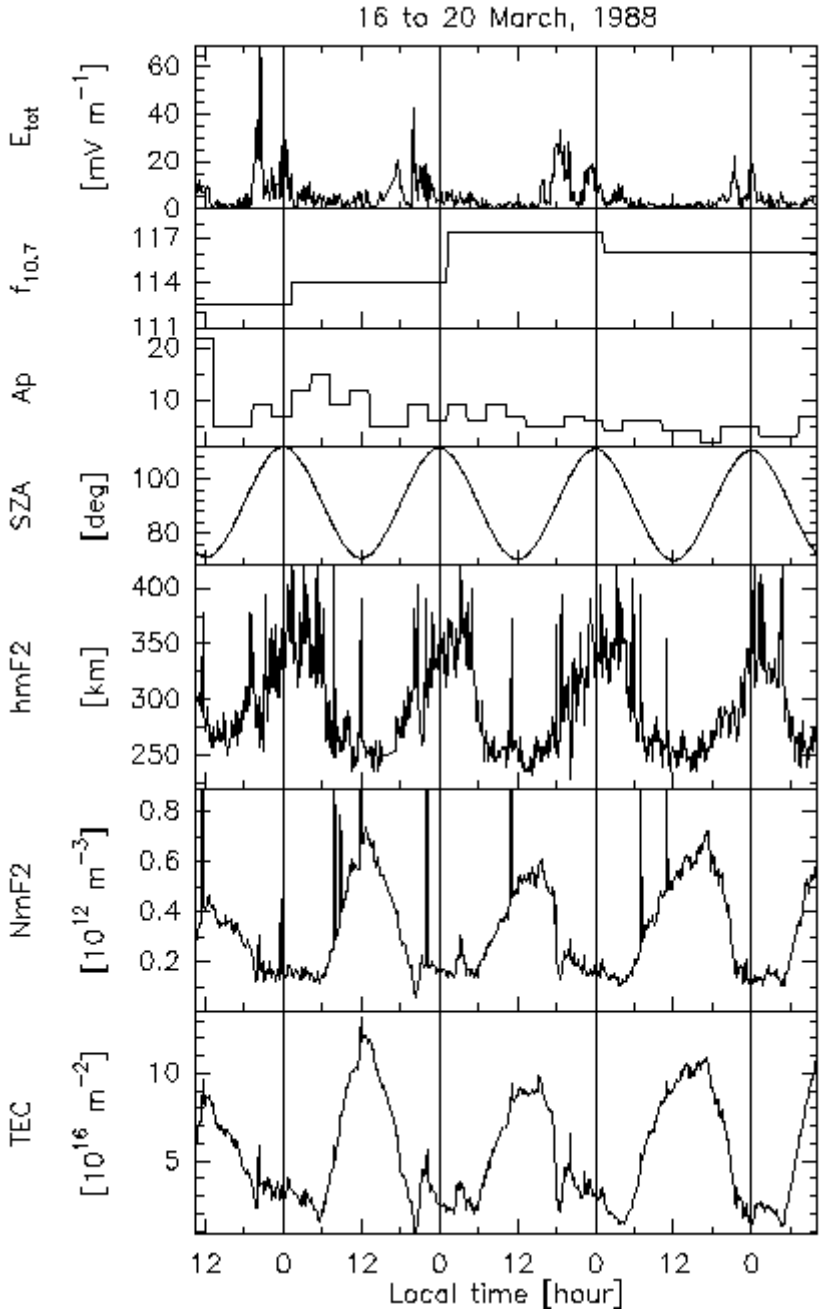

Figure 6: Same as Figure 1 for the experiment held from the 16 to the 20 March 1988.

However, one must be very careful with such a simple law. Its only purpose is to give an idea of the mean ITEC behaviour. First of all, one must use the decimetric index with

caution for instantaneous laws, since this index is a daily index. Then, equation 13 is fitted from EISCAT data, and cannot be a priori used for lower latitudes. The 1/15 factor certainly depends on the neutral atmosphere: together with the hyperbolic tangent, it is a very simple representation of a corrected Chapman function, which depends on the atmosphere along the line of sight. It also depends on the atmosphere through photoionization, which is a function of the neutral concentrations. Finally the 1/15 factor depends on the coefficient rates, which are functions of the temperatures. Since the neutral atmosphere varies with latitude, this 1/15 factor may well be different at different latitudes. Equation 13 has also been established using only quiet magnetic and electric conditions. The fitting procedure does not give reasonable values of A and B as soon as magnetic storm conditions occur. Finally, it is computed for height integration up to 425 km only. In a companion paper (Lilensten and Blelly, 2001), we show from a model that when the electron density is integrated up to 3000 km, the ITEC is about 2 times bigger than when the electron density is integrated only up to 425 km. Finally, in several cases, this law is not satisfying. As an example on March 17 to 20, 1988 (Figure 6), an increase of the solar activity (114 to 117) corresponds to a decrease of the noon electron content (12 to 9 10^{16}). At that time, there are no electric fields and no evidence of particle precipitation, but there is a large solar illumination ($\chi < 76°$ at noon).

Those points explain why neural networks or non-linear schemes are useful at predicting the TEC or foF2 (Wintoft and Cander, 1999, and references herein). But it is important to notice that these models need good calibrated inputs, especially at high latitude where the EISCAT facility constitutes a unique tool.

In spite of those warnings, equation 13 may be of some use for the estimation of a global mean behaviour of the electron content at high latitude. In the same way, we have performed a similar calculation on NmF2. The results are plotted in Figure 7. The upper panel shows the ratio:

$$\frac{\mathrm{NmF2}\ 10^{-12}}{\sqrt{f_{10.7}\ \cos\chi}} = \mathrm{R1'} \qquad (14)$$

and the middle panel the ratio:

$$\frac{\mathrm{NmF2}\ 10^{-12}}{f_{10.7}\ \cos\chi} = \mathrm{R2'} \qquad (15)$$

The dependence of NmF2 on the direct product $f_{10.7}\ \cos\chi$ or to its square root is not easy to distinguish. This is because the altitude of NmF2 during sunlight times is often around 180 to 250 km, which represents the transition altitude between the two laws. At night, hmF2 sometimes exceeds the upper measurement altitude (425 km) and therefore, NmF2 is very poorly estimated. This never happens during sunlight periods: hmF2 is usually below 350 km and NmF2 is then correctly measured.

In order to stay coherent with the fit of the ITEC, we have chosen to perform a fit on R2'. The result of this fit is plotted in the middle panel of Figure 6. However, the dispersion of NmF2 is larger than the dispersion of the ITEC, and we had to remove several observations in order to reach a good standard deviation in the procedure. In order to make our selection, we have computed the standard deviation of R2' (called $\sigma_{R2'}$), and we have kept the points around the average $\pm\ 0.4\ \sigma_{R2'}$.

In Figure 7, we show all the points, even those that have been excluded. With the same warnings as for the ITEC, we can write the following modelling of NmF2:

$$10^{-12}\ \mathrm{NmF2} = \frac{1}{250}\,\frac{f_{10.7}\ \cos\chi}{\tanh\left(\pi/2 - \chi\right)} \qquad (16)$$

Here, NmF2 is in m^{-3}. The standard deviation of the 250 factor is 0.11. The ratio between this factor (250) and the factor in the equation 13 (15) represents of course the average between the ITEC and the NmF2 values over all the experiments. The true ratio, when all the experiments are kept, is 19 instead of 16.7 here. The bottom panel in Figure 7 shows the error defined as the ratio $R2'(\chi)/R',\hat{}2(\chi)$. It is again relatively small, at least for the points that have been used in the fitting procedure.

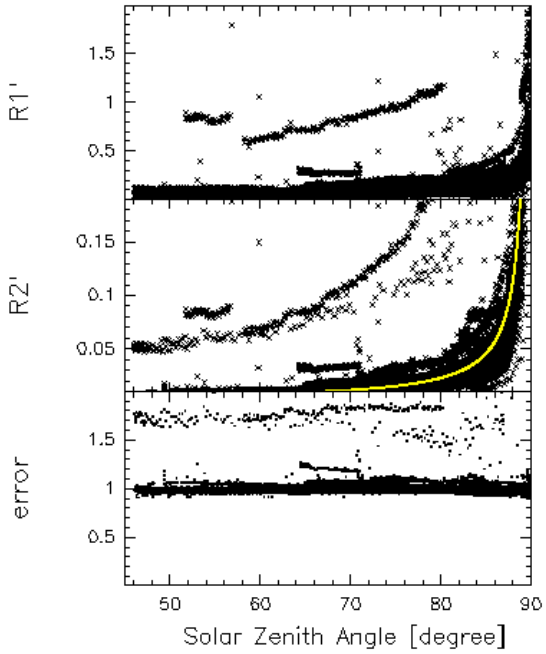

Figure 7: Same as Figure 5 for NmF2 data

The values of hmF2 during quiet electric and magnetic conditions are much more variable than the values of the ITEC and even of NmF2 during sunlight conditions (see Figures 2 or 6 as examples). This is because the high latitude ionosphere is very dynamic and moves the F-layer up and down by a few kilometres to a few tens of kilometres. For solar angles below 90°, it very occasionally exceeds 425 km: it is almost always constrained between 220 km and 360 km. At night, it often exceeds the upper limit of our power profile measurement. The effect of particle precipitation is very well seen in Figure 7 at solar angles larger than 90°. It can lower NmF2 to 160 km, even during these quiet periods.

There is however a characteristic of the electron behaviour that does not depend on the activity level. The ITEC and the NmF2 are not symmetric around noon. In this study, we have selected all the days with no evidence of any precipitation or electric field and with solar illumination at noon. This data set covers a large range of magnetic and solar activity conditions. We have then measured the width of the ITEC and of the NmF2 around noon at mid-height, and computed the ratio between the morning and evening component of this width. This ratio represents the morning/afternoon asymmetry. It has an average of 0.73

(same value for the ITEC and for NmF2) with a standard deviation of 0.1, i.e. the electron content of the ionosphere decreases slower in the afternoon than it increases in the morning. This pattern is due to the neutral atmosphere composition, which is not symmetric around noon. Figure 1 shows two good examples of this width variation, which can of course not be well reproduced by equation 13 or by equation 16.

Effect of the electric field

The diurnal ionization is mostly due do the solar photoionization. However, the behaviour of the ionosphere is influenced by the presence of an electric field. In Figure 8, we have plotted the EISCAT deduced ITEC (in the same format as in Figure 5) when the electric field is larger than 30 mV m^{-1}. The grey line in the middle panel corresponds to the law fitted with electrically quiet data (equation 13). In the bottom panel, we show the error made when this law is used on these active condition data. Since the shapes of R2 or R1 are close to what they are in electrically quiet data, it would be in principle possible to proceed to a new fit. This however would be physically meaningless because all the values of the intensity of the electric field would be mixed. Unfortunately, the database is not large enough to allow a study of a large set of different electric field conditions.

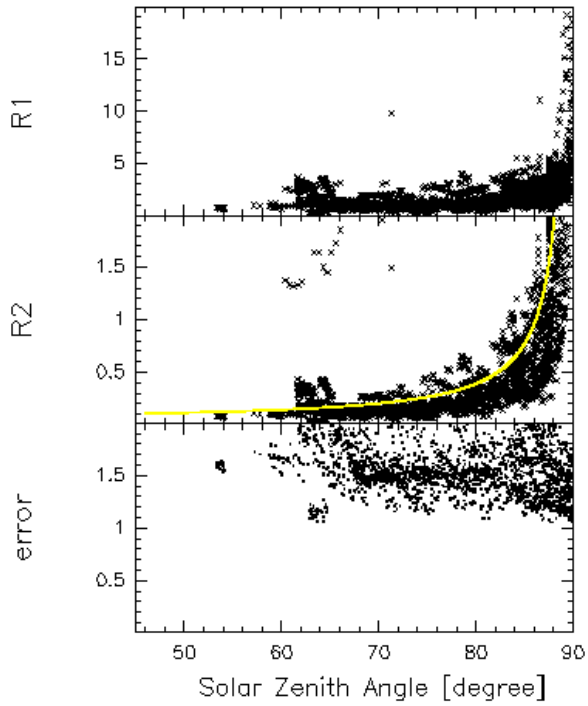

Figure 8: Same as Figure 5 (for TEC data), but with data acquired during electrically perturbed conditions. The line is the law fitted on quiet time data (same as in Figure 5). The errors in the bottom panel are between the data in the middle panel and this quiet time condition law

This reaction produces NO^+, and has several coefficient rates depending on the excitation states of the initial and final ions. However, the most important reaction is $O^+ (^4S)+N_2 \rightarrow NO^+ + N$ which has a reaction coefficient of:

$$\begin{cases} 1{,}533\ 10^{-18} - 5{,}92\ 10^{-19}\left(\frac{T_r}{300}\right) + 8{,}6\ 10^{-20}\left(\frac{T_r}{300}\right)^2 & 300 \le T_r \le 1700\ K \\ 2{,}73\ 10^{-18} - 1{,}155\ 10^{-18}\left(\frac{T_r}{300}\right) + 1{,}483\ 10^{-19}\left(\frac{T_r}{300}\right)^2 & 1700 \le T_r \le 6000\ K \end{cases} \quad (17)$$

where Tr is the reduced temperature equal to the average between neutral and ion temperatures. The enhancement of the ion temperature thus produces more NO^+, which recombines with e- through dissociative recombination:

$$NO^+ + e^- \rightarrow N + O \qquad kr = 4.2\ 10^{-13}\left(\frac{Te}{300}\right)^{-0.85}\ m^{-3}\ s^{-1} \quad (18)$$

The effect is to depopulate the ionosphere at altitudes below typically 250 km. Schunk and Nagy underlined the fact that for electric field strengths less than about 10 mV/m, the depletion of O+ is small, and the altitude profiles of ion density are similar to those found at mid-latitudes. However, for moderate electric field strengths (50 mV/m), NO^+ is substantially increased in relation to O^+ and becomes an important ion throughout the F-region. They note an additional effect of the consequent perpendicular -E x B drifts. For large electric fields (200 mV/m), NO^+ completely dominates the ion composition to at least 600 km, decreasing at high altitudes with a diffusive equilibrium scale height. Since the overall F region electron density decreases markedly with increasing electric field strength, it appears that high-latitude; daytime electron density troughs are directly related to the presence of ionospheric electric fields.

Since the effect of the electric field is mostly important at altitudes where the ITEC obeys a

$1/\sqrt{f10.7\ \cos\chi}$ law, it is not surprising that the excursion of R1 is smaller when electric field is present: hmF2 increases and the electron population becomes more directed by a $1/(f10.7\ \cos\chi)$ law.

Magnetic storm effects on specific cases

Geomagnetic storms are intervals when a sufficiently intense and long lasting interplanetary convection electric field leads to an intensified ring current. The exact frontier between storm and sub-storm is still unclear (Gonzalez et al., 1994). It is observed that when the electric field at high latitude exceeds typically 20 $mV.m^{-1}$, there is weak precipitation. This is probably because the ring current grows until some key threshold of the quantifying index Dst is exceeded. Their effects on the electron density are known, and will be shown below. The ITEC behaviour during the geomagnetic storm of January 10, 1997 has been investigated by Jakowski et al. (1999) over Europe and three North American stations at latitudes ranging from 65° to 35°, while the F2 layer was studied for the same period by Mikhailov and Förster (1999). Here, we want to emphasize it over a large period including several storms at high latitude only.

Before this effect is studied, one must emphasize what electric field the radar measures. It is the superposition of the effective electric field in the neutral gas frame i.e. $\mathbf{E_{eff}}$, and an additional electric field component. The latter is due to the presence of a magnetic field, which creates a $\mathbf{v_N}x\mathbf{B}$ electric field (where $\mathbf{v_N}$ is the vector neutral velocity and $\mathbf{B}$ the magnetic field):

$$\mathbf{E} = \mathbf{E_{eff}} - \frac{1}{c}\mathbf{v_N}x\mathbf{B} \quad (19)$$

This may adversely affect the observation.

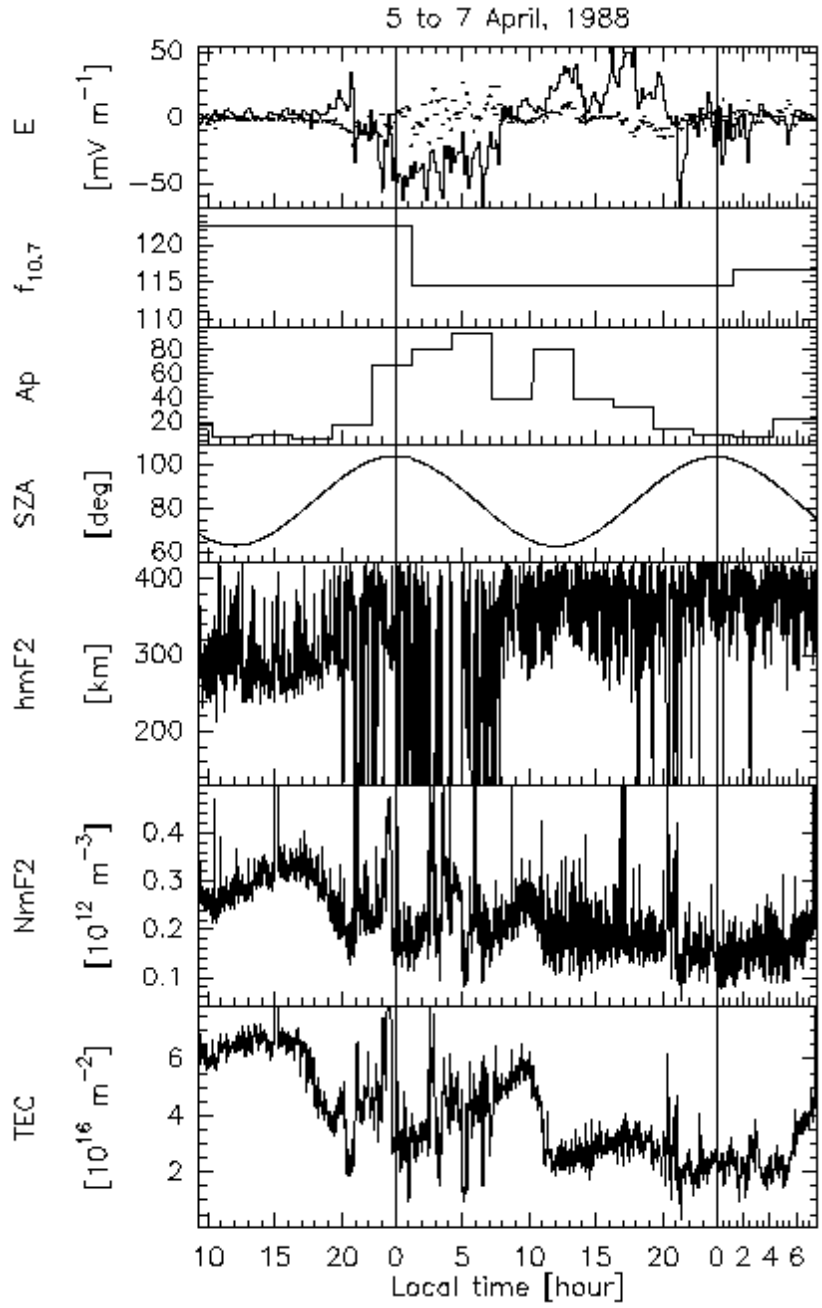

Figure 9: Same as Figure 1 for the experiment held from the 5 to the 7 April 1988. In the upper panel, the line shows the northward component of electric field (positive to the north) and the dots show the eastward component (positive to the east).

In addition to the chemical effect discussed above, there are several effects of an electric field. They are summarized in Kelley (1989) and Lilensten and Blelly (2000). It creates a frictional heating of the ions due to the perpendicular electric field. It implies an anisotropy of the plasma, and a modification of the ion composition. This effect is important above 30 mV.m^{-1} (Lathuillère et al., 1997). At 65 mV.m^{-1}, the transition altitude (at which molecular and atomic ions are in equal concentration) increases from 215 to 255 kilometers.

This is particularly obvious in an experiment such as the 5 to 7 April 1988 (Figure 9). The Ap index reaches values larger than 80, indicating the presence of a magnetic disturbance.

In Figure 9, we have plotted both the northward and eastward electric field components. The two components remain small until about 18 LT on the first day. It then experiences a strong enhancement to the north (with a small westward component) and then around 22 LT turns southeast. The southward component reaches 60 $mV.m^{-1}$ but remains large all night. At 8 LT the second day, the electric field turns northward again with large values (up to 50 $mV.m^{-1}$). We focus on this northward enhancement. The solar zenith angle reaches values of 70°, with a decimetric index of 115. The electron density is then increasing due to solar photoionization. When the northward component of the electric field passes about 15 $mV.m^{-1}$, the electron content suddenly decreases and remains low during the whole storm, for the rest of the day. This behaviour is very well illustrated in those partial parameters.

The database allows returning to the height profiles. In Figure 10, we show the EISCAT measurements during this whole experiment. Naturally, all the patterns in the ITEC and foF2 parameters can be retrieved. The important thing in this discussion is the enhancement of the ion temperature on 6 April, lasting until the end of the experiment, while the strong electron precipitation more or less stops around 10 UT. The ion temperature reaches values larger than 2000 K.

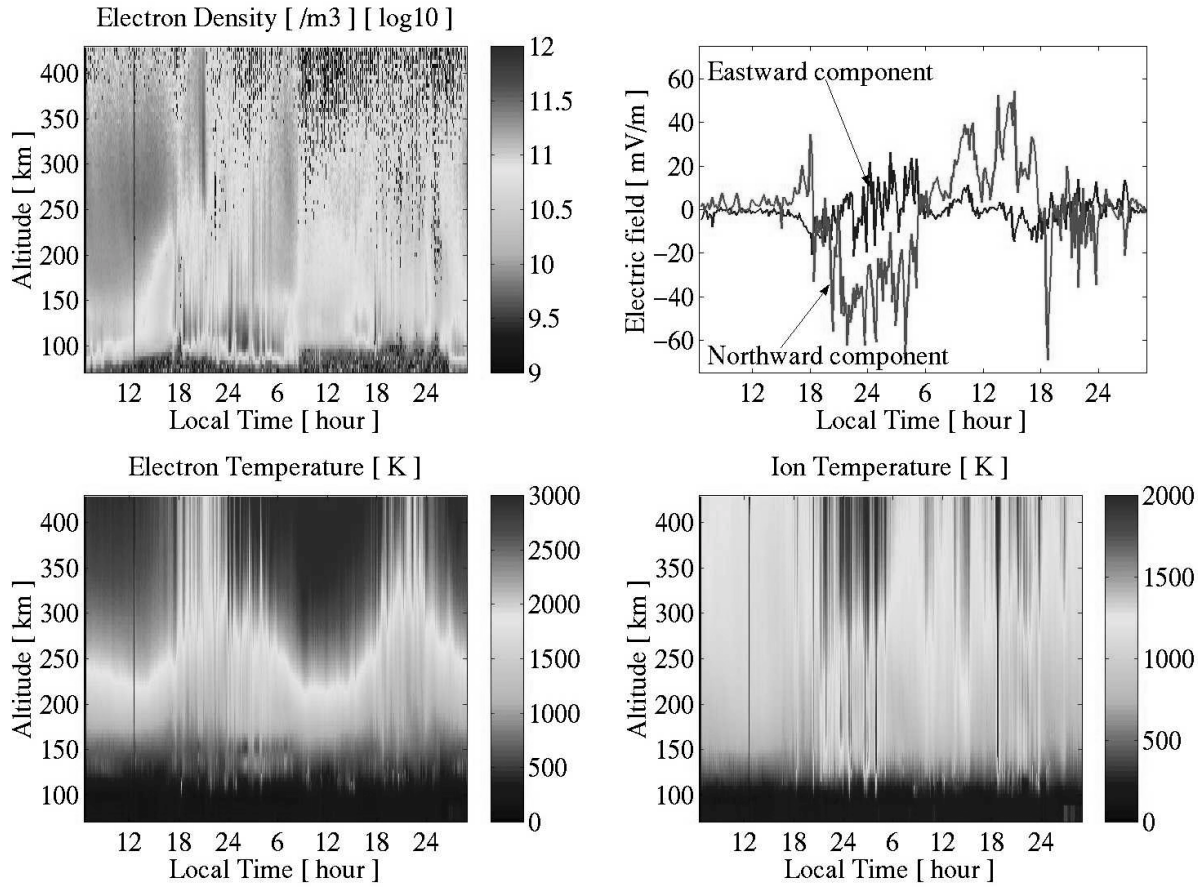

Figure 10: The basic parameters measured by the EISCAT radar, during the same experiment as shown in Figure 9, namely the electron density, electric fields, electron, and ion temperatures (the ion velocity is not shown here).

In the whole data set, we see no evidence of the Harang discontinuity on any of the 3 studied parameters. This is because when the electric field turns to the north, its value is small.

Another spectacular experiment was held 2 years later, from 9 to 10 April 1990 (not shown here). On these days, the decimetric index is about the same (150/145) and another magnetic storm occurs (Ap reaches values of 200). The photoionization only compensates the electric field effect for solar zenith angles smaller than 65°. Such effects have been studied on large scales (Kutiev et al., 1998) in order to make forecasts for space weather purposes (Candler and Mihaijlovic, 1998).

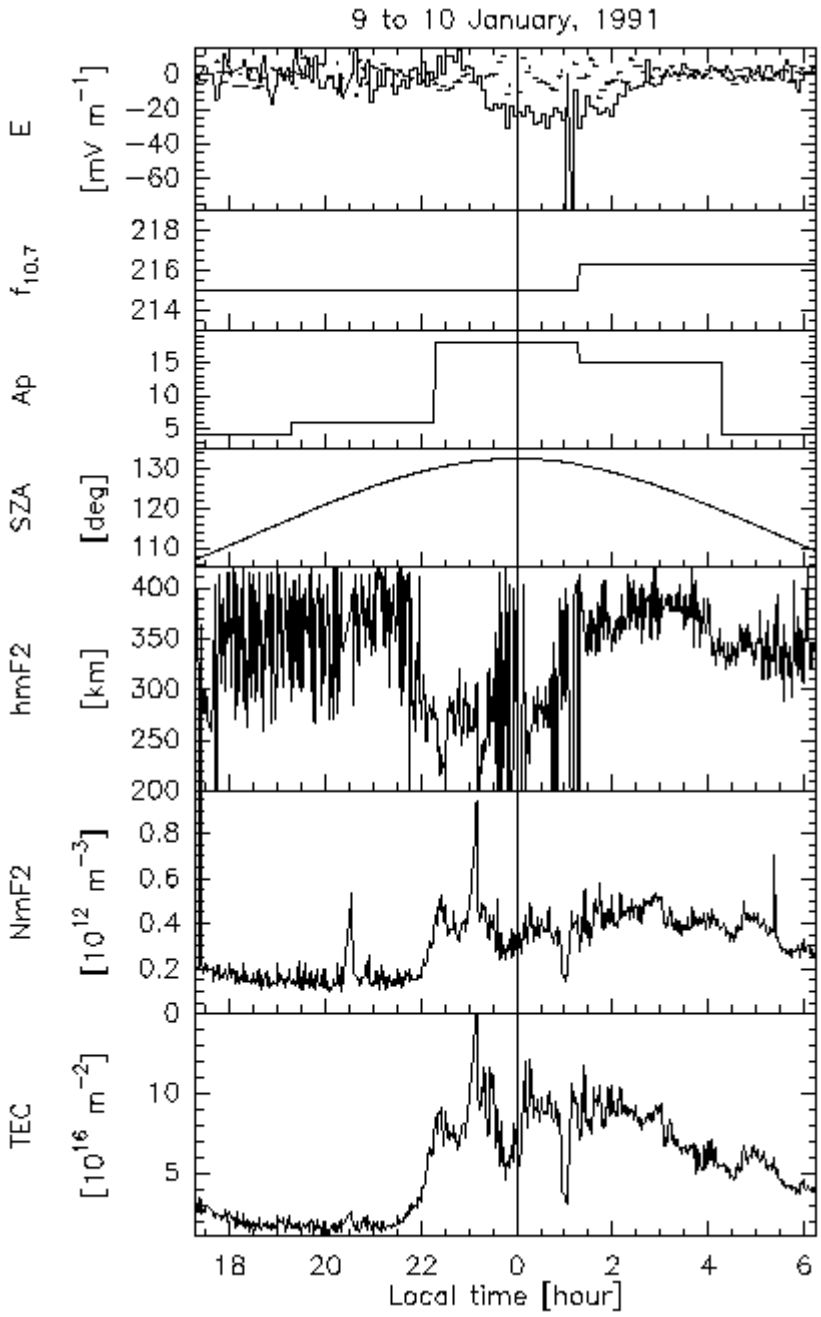

Figure 11: same as Figure 9 for the experiment held from the 9 to 10 January 1991.

Effect of particle precipitation

In Figure 1, the precipitation occurs around midnight (local time) on the two days. Not surprisingly, the electrons are enhanced. When the precipitation is soft, such as at 20 LT on the first day, the maximum of the F region decreases from 340 to 300 km, but most of the time, the precipitation has an effect on the E region, so that hmF2 is not affected. In Figure 11, we show a night time experiment, from 9 to 10 January 1991. Until 21.30 LT, the ionosphere is rather empty. The precipitation occurs at 22 LT, enhancing the electron content up to 1.5 m^{-2}. The altitude of the F maximum decreases to 150 km, demonstrating a soft electron flux of about 1 keV at midnight.

Effect of an arc

We often have competition between the electric field and precipitation. This usually does not occur during strong storms, but mostly for electric fields below typically 20 $mV.m^{-1}$. In Figure 11, it is the case at 1 LT the second day of the experiment, when the southward electric field suddenly amounts to 75 $mV.m^{-1}$. The electrons experience a sharp decrease, soon followed by an increase under the effect of the precipitation, although the field remains important for the next hour (about 20 $mV.m^{-1}$).

However, in many cases, what is seen is well illustrated in Figure 1. On each of the 3 days, there is an electric field event (at 18 LT on 17 November, at 20 LT on 18th, and at 15 LT on the 19th) soon followed by strong particle precipitation that compensates for the electric field driven reduction of the ITEC and NmF2. This is particularly drastic on 18 November, since the total electric field reaches values of 70 $mV.m^{-1}$ for a short time. This behaviour is seen more than 20 times on the database, and is the signature of arcs for which the electric field shortly precedes the electron precipitation. This is also quite spectacular in Figure 6 the 3 first days around 20 LT: when the electric field passes 20 $mV.m^{-1}$, the electron content drops down. The same occurs on the 5 April 1988 (Figure 9) shortly after 20 LT. Soon after the electric field enhancement, the precipitation starts. The particle precipitation is also visible on the electron density on the upper left panel of Figure 10.

The structures of the arcs have been discussed at length (Akasofu and Kan, 1981) and recent measurements inside the arcs themselves show that they are highly variable in space as in time (Marklund et al., 1998). However, the structure presented here, seen on many experiments, seems to be a very common one.

Conclusion

We have examined a database of EISCAT covering more than one solar cycle of measurements. Although it contains thousands of hours of measurements, the necessity of electric field values reduces the usable data to 1260 hours. The experiment from 30 July to 5 August 1992 is a good summary of our study (Figure2). It is a sunlight experiment with maximum zenith angles of 92°. The decimetric index gradually increases from 100 to 134, and the total electron content follows this increase: from 9 10^{16} m^{-3} at noon the second day to 12 10^{16} m^{-3} the sixth day. At night, on the second and fourth days (1 and 3 August), there are mean electric field periods (about 20 $mV.m^{-1}$). They result in an initial decrease in the electron concentrations both in the ITEC and NmF2, soon followed by particle precipitation. This is a typical signature of an electric arc. Finally, a sub-storm occurs the last day with values of the southward electric field reaching 80 $mV.m^{-1}$. As a result, the ions are heated and rapidly recombine with the atmosphere. The ionosphere is emptied, with ITEC values of less than 0.3 m^{-2}.

The purpose of this technical report is to illustrate the use of EISCAT a tool for Space Weather studies, in particular in contributing to the knowledge of the high latitude TEC, Nmf2, and hmF2. These 3 parameters are the only ones to be routinely measured over large geographic area by the use of ionosondes and GPS signals.

It capitalises on two actions. First, an update of the EISCAT data base. Then, a recommendation of the international ITU-R committee to use EISCAT as a Space Weather facility. We now consider these in more detail.

The EISCAT data base

This site is associated with the C.D.P.P. (Centre des Données de la Physique des Plasmas), a data archiving and distribution centre for Space Plasma Physics, implemented by the C.N.R.S. (Centre National de la Recherche Scientifique), and the C.N.E.S. (Centre National d'Etudes Spatiales). Its URL is http://www-eiscat.ujf-grenoble.fr/. It archives the ionospheric data from the EISCAT radar, which have been analyzed in France, from 1981 to 1999 with the TAPANAL processing code (Lathuillère and Pibaret, 1992). The data are given both in GIF or ASCII formats. Following the present work, an upgrade of the data base has been performed in order to include the ITEC, f0F2, NmF2, and hmF2 data (Lemieux-Dudon, 2003). The parameters are given up to 600 km using both the single and the multipulse.

ITU-R recommendation

The International Telecommunication Union (ITU) is an international organization within the United Nations system where governments and the private sector coordinate global telecom networks and services. It includes three working groups: Telecom Standardization (ITU-T), Telecom Development (ITU-D), and Radio-communication (ITU-R). The ITU-R plays a vital role in the management of the radio-frequency spectrum and satellite orbits. These finite natural resources are increasingly in demand from a large number of services such as fixed, mobile, broadcasting, amateur, space research, meteorology, global positioning systems, environmental monitoring and, last but not least, those communication services that ensure safety of life at sea and in the skies. All these uses depend on space weather conditions, especially at high latitude.

The present study has been used as a basis for the ITU-R group on « Ionospheric propagation data and prediction methods required for the design of satellite services and systems ». It issued a recommendation on a proposed data bank for Transionospheric model testing (recommendation 531-6, June 2002). For this purpose, this recommendation explicitly proposes EISCAT as the major facility.

Acknowledgements

We are grateful to Chantal Lathuillère for comments on this work. EISCAT is an International Association supported by the Research Councils of Finland (SA), France (CNRS), the Federal Republic of Germany (MPG), Japan (NIPR), Norway (NFR), Sweden (VR), and the United Kingdom (PPARC).

Bibliography

Akasofu S.I. and J.R Kan, 1981, Physics of auroral arc formation, Geophysical monographs, AGU Series, Wash. DC.

Altinay O., E. Tulunay and Y. Tulunay, 1997, Forecasting of ionospheric critical frequency using neural networks, *Geophys. Res. Lett.*, **24**, 1467-1470

Banks, P.M., and G. Kockarts, 1973, Aeronomy, part A and B, Academic Press, New-York.

Bauer, P. , 1975, Theory of waves incoherently scattered, *Phil. Trans. R. Soc. Lond, A*, **280**, 167-191

Bilitza D., N. Papitashvili and J. King, 2001, IRI related data and model services at NSSDC, *Adv. Space Res.*, **27**, 131-141

Cander Lj. R. and S.J. Mihajlovic, 1998, forecasting ionospheric strucutre during the great geomagnetic storms, *J. Geophys. Res.*, **103**, 391-398

Chapman, S., 1931, Absorption and dissociative or ionising effects of monochromatic radiation in an atmosphere on a rotatin earth, *Proc. Phys. Soc., London,* **43**, 1047-1055

Codrescu M.V., S.E. Palo, X. Zhang, T.J. Fuller-Rowell, C. Poppe, 1999, TEC climatology derived from TOPEX/POSEIDON measurements, *Journal Atmos. Solar-Terre. Phys.*, **61**, 281-298

Das Gupta, A., S. Basu,; J. N. Bhar, and J. C. Bhattacharyya, Ionospheric electron content and equivalent slab thickness in the equatorial region, Journal of Geophysical Research, **80**, 699-701,1975

Gonzalea W.D., J.A. Joselyn, Y. Kamide, H.W. Kroehl, G. Rostoker, B.T. Tsurutani and V.M. Vasyliunas, 1994, What is a geomagnetic storm ?, *J. Geophys. Res.*, 99, 5771-5792

Green, A.E.S., Lindenmeyer and Griggs, 1964, Molecular absorption in planetary atmosphere, *J. Geophys. Res.*, **69**, 493-504

Hagfors, T., 1997, Plasma fluctuations excited by charged particle motion and their detection by weak scattering of radio waves, *Incoherent scatter, theory, practice and science,* D. Alcaydé Ed., Technical report 97/53, EISCAT scientific association

Hedin, A.E. , 1991, Extension of the MSIS thermosphere model into the middle and lower atmosphere, *J. Geophys. Res.*, **96**, 1159-1172

Iijima B.A., I.L. Harris, C.M. Ho, U.J. Lindqwister, A.J. Mannucci, X. P, M. J. Reyes, L.C. Sparks, and B.. Wilson, 1999, automated daily porcess for global ionospheric total electron content maps and satellite ocean altimeter ionospheric colibration based on Global Positioning System data, *Journal Atmos. Solar-Terre. Phys.*, **61**, 1205-1218

Jakowski N., Sardon E., E. Engler, A. Jungstand and D. Klähn, relationships between GPS signal propagation errors and EISCAT observations, *Ann. Geophys.*, **14**, 1429-1436, 1996

Jakowski N., Sardon E., and S. Schlutter, GPS-based TEC observations in comparison with IRI95 and the European TEC model NTCM2, *Adv. Space. Res.*, **22**, 803-806, 1998

Jakowsky N., S. Schlutter, and E. Sardon, 1999, Total electron content of the ionosphere during the geomagnetic storm on January 10, *J. Atmos. Terr. Phys.*, **61**, 299-308, 1997

Jakowski, N.; Fichtelmann, B.; Jungstand, A., Solar activity control of ionospheric and thermospheric processes, *J. Atmos. Terr. Phys.*, **53**, 1125-1130, 1991

Kelley M.C., 1989, The Earth's Ionosphere, Plasma physics and electrodynamics, Academic Press Inc., ISBN 0-12-404013-6

Komjathy A., Langley R. B. and D. Bilitza, 1998, ingesting GPS-derived TEC data into the international refernce ionosphere for single frequency radar altimeter ionospheric delay corrections, *Adv. Space. Res.*, **22**, 793-801

Kouris S., D.N. Fotiadis, and T.D. Xenos, 1998, one the day to day variation of foF2 and M(3000)F2, *adv. Space Res.*, **22**, 873-876

Kutiev I., P. Muhtarov and P.A. Bradley, 1998, Penetration of ionospheric disturbances nto the european region during geomagnetic storms, *Adv. Space Res.*, **22**, 865-867

Lathuillère C. and B. Pibaret, A statistical model of ion composition in the auroral F-region, *Adv. Space Res.*, **12**, 147-156, 1992

Lathuillère C. , P.L. Blelly, J. Lilensten and P. Gaimard, 1997, Storm effects on the ion composition, *Advanced and Space Research*, **20**, 1699-1708

Lemieux-Dudon B., W. Kofman, C. Lathuillère, J. Lilensten, P. Pibaret and P. Volcke, Additional "space weather data" in the brand new Grenoble EISCAT database, communication to the EISCAT Workshop, 2003.

Lilensten, J., W. Kofman, J. Wisemberg, E.S. Oran, and C.R. DeVore,1989, Ionization efficiency due to primary and secondary photoelectrons:A numerical model, *Ann. geophysicæ*, 7, 83-90

Lilensten J. and P.L. Blelly, Du Soleil à la Terre, aéronomie et météorologie de l'espace, collection Grenoble Sciences, PUG, ISBN 2 7061 0834 7, 2000

J. Lilensten and P.L. Blelly, The TEC and F2 parameters as tracers of the ionosphere and thermosphere, JASTP, **64**, 775-793, 2002

Marklund G.T., T. Karlsson, L.G. Blomberg, P. A. Lindqvist, C.G. Fälthammar, M.L. Johnson, J.S. Murphree, L. Andersson, L. Eliansson, H.J. Opgenoorth, and L. J. Zanetti, 1999, Observations of the electric field fine structure associatied with the westward traveling surge and large scale auroral spirals, *J. Geophys. Res.*, **103**, 4125-4144

McNamara, L. F. and P. J. Wilkinson, Prediction of total electron content using the International Reference Ionosphere, *J. Atmos. Terr. Phys.*, **45**, 169-174, 1983

Mikhailov A.V. and V. V. Mikhailov, 1995, A new ionospheric index MF2, *Adv. Space. Res.*, 93-97

Mikhailov A.V. and M. Förster, 1999, Some F2-layer effects during he January 6-11 1997 CEDAR storm period as observed with the Millstone Hill incoherent scatter facility, *Journal Atmos. Solar-Terre. Phys.*, **61**, 249-262

Newell, P.T., and C.I. Meng, 199 Ionospheric projections of magnetospheric regions under low and high solar wind pressure conditions, *J. Geophys. Res.*, **99**, 273-2864

Perrone L. and G. de Franceschi, 1999, a correlation stydy between time-weighted magnetic indices and the heigh latitude ionosphere, *Phys. And Chem. Of the Earth*, **24**, 389-392Richard, P.G., and D.G. Torr, 1988, Ratio of photoelectron to EUV ionization rate for aeronomic studies, *J. Geophys. Res.*, **93**, 4060-4066

Rishbeth, H. and A. P. Van Eyken, 1993, EISCAT : early history and the first ten years of operation, *J. Atmos. Terr. Phys.*, **55**, 525-542

Rush C., D. Miller, qnd J. Gibbs, 1974, the relative daily variability of foF2 and hmF2 and their implications for HF radio propagation, *Radio Sci.*, **9**, 749-756

Schunk, R. W.; Banks, P. M.; Raitt, W. J., Effect of electric fields on the daytime high-latitude E and F regions, *J. Geophys. Res.*, **80**, 3121-3130, 1975

Sheehan, C. H., A merged beam analysis of the dissociative recombination of molecular ions of importance to ionospheric and interstellar chemistry, Thesis (PhD)., Univ. West. Ontario (Canada), 2001

Smithe and Smith, 1972, Numerical evaluation of Chapman's grazing incidence integral ch(X,x), *J. Geophys. Res.*, **77**, 3592-3597

Stanislawska I., G. Juchnikowsky, R. Hanbaba., Lj. R. Cander, Z. Klos and Z. Zbyszynski, 1998, an automatic system for HF propagation conditions prediction and forecast, 2nd COST 251 workhop proceedings, ed. A. Vernon, RAL, UK ernon, 294-297

Wahlund, J.-E., H. J. Opgenoorth, I. Häggström, K. J. Winser, 1992, and G. O. L. Jones, EISCAT Observations of Topside Ionospheric Ion Outflows during auroral activity : Revisited, *J. Geophys. Res.*, **97**, 3019-3037

Wintoft P. and L. Cander, 1999, Short-term predictions of fof2 using time-delay neural network, *Phys. and Chem. of the Earth*, **24**, 343-347